Bound Pairs of Fronts in a Real Ginzburg-Landau Equation Coupled to a Mean Field

Henar Herrero
Departamento de Física y Matemática Aplicada, Facultad de Ciencias
Universidad de Navarra, 31080 Pamplona, Navarra, Spain

Hermann Riecke
Department of Engineering Sciences and Applied Mathematics
Northwestern University, Evanston, IL 60208, USA

Motivated by the observation of localized traveling-wave states ('pulses') in convection in binary liquid mixtures, the interaction of fronts is investigated in a real Ginzburg-Landau equation which is coupled to a mean field. In that system the Ginzburg-Landau equation describes the traveling-wave amplitude and the mean field corrsponds to a concentration mode which arises due to the slowness of mass diffusion. For single fronts the mean field can lead to a hysteretic transition between slow and fast fronts. Its contribution to the interaction between fronts can be attractive as well as repulsive and depends strongly on their direction of propagation. Thus, the concentration mode leads to a new localization mechanism, which does not require any dispersion in contrast to that operating in the nonlinear Schrödinger equation. Based on this mechanism alone, pairs of fronts in binary-mixture convection are expected to form *stable* pulses if they travel *backward*, i.e. opposite to the phase velocity. For positive velocities the interaction becomes attractive and destabilizes the pulses. These results are in qualitative agreement with recent experiments. Since the new mechanism is very robust it is expected to be relevant in other systems as well in which a wave is coupled to a mean field.

submitted to Physica D, August 8, 1994

I. INTRODUCTION

Among the most striking recent findings in the investigation of pattern-forming dissipative systems have been the observations of stable *localized* structures surrounded either by the structureless basic state or by other structures. Steady structures of this kind have been found in experiments on Rayleigh-Bénard convection in narrow channels where patches of rolls with long wavelength coexist with patches of short wavelength [1–3]. In Taylor vortex flow large, turbulent axisymmetric vortices have been found to coexist stably with small, laminar vortices [4]. Another class of localized structures is given by the localized drift waves observed in a variety of systems undergoing a parity-breaking bifurcation. They were first found in directional solidification [5]. Subsequently they were also observed in other interface instabilities like the printer instability [6] and in cellular flames [7]. Based on theoretical predictions [8], the same phenomena were then found in Taylor vortex flow between counter-rotating cylinders [9]. Theoretically, these localized drift waves have been successfully described with phase-amplitude equations adequate for a parity-breaking bifurcation [8,10–16].

The present paper is motivated by localized waves which have been observed in the convection of binary mixtures. They consist of traveling-wave packets ('pulses') which drift through the conductive, structureless state. They have been investigated in great detail and presumably constitute the best studied structures of this kind [17–21]. Depending on parameters, two seemingly different classes of pulses have been found. For weakly negative separation ratio ψ of the mixture the pulses comprise only a few wavelengths and their size is relatively independent of the parameters (pulses of 'fixed width'). For more negative values of the separation ratio long packets have been observed. In early experiments their width varied from run to run in a seemingly random manner (pulses of 'arbitary width'). In those experiments both types of pulses were stationary, with the convection rolls traveling through the pulse. In numerical simulations of the Navier-Stokes equations [22,23] and in subsequent improved experiments it was found that the short pulses [20] and then also the long pulses [24] in fact drift as had been expected on general symmetry grounds. The drift velocity was, however, found to be extremely small.

Analytically, these pulses have been described within the framework of a complex Ginzburg-Landau equation. Two approaches have been taken. In the strongly dispersive limit the Ginzburg-Landau equation can be viewed as a dissipatively perturbed nonlinear Schrödinger equation and it has been shown that the pulses can arise from the solitons of that equation [25–28]. For weak dispersion localized waves have been described by fronts which can form stably bound pairs due to the repulsive interaction arising from the dispersion [29,30]. In either case, the localized waves should travel with a velocity which is essentially given by the linear group velocity of the waves. The experimentally and numerically observed velocity is, however, by a factor of 20 to 30 smaller [20,22]. In addition, the numerical simulations revealed a striking behavior of the concentration field, which is advected by the traveling rolls. It was suggested that it could be respon-

sible for the slow-down of the pulses [22]. This finding motivated a detailed analysis of the derivation of the conventional Ginzburg-Landau equations. It was shown that these equations break down already quite close to threshold; due to the slow mass diffusion in liquids, which is characterized by their small Lewis number $\mathcal{L} = O(10^{-2})$, certain modes of the concentration decay very slowly and have to be treated as independent dynamical variables in addition to the convective amplitude A [31–33]. For free-slip-permeable boundary conditions extended Ginzburg-Landau equations for A and a large-scale concentration mode C have been derived. In contrast to the conventional Ginzburg-Landau equation, they do not become singular in the limit $\mathcal{L} \to 0$ and constitute a minimal model to describe this important physical effect.

Numerical simulations of the extended Ginzburg-Landau equations in the strongly dispersive case showed that the concentration field can indeed slow down the pulses considerably [31–33]. Analytical investigations using soliton perturbation theory confirm this result [33,34]. Numerically, it has also been found that (long) pulses can arise stably even *without dispersion* when the concentration mode is included [31,32]. This shows, that in this system a second mechanism, which is unrelated to that responsible for the solitons of the nonlinear Schrödinger equation, may be able to induce the localization of waves. In the present communication we discuss long pulses considering them as a bound pair of fronts. We isolate their localization mechanism analytically and show that the interaction between fronts can become *repulsive* if the pulse travels *backward*, i.e. opposite to the velocity of the waves. This mechanism is quite robust and may be expected to be relevant in other systems as well. Equations similar to those discussed here have been derived, for instance, for two-fluid channel flow [35].

Recently, the interaction of fronts in a system of reaction-diffusion type with two fields has been investigated [36]. In that work stably bound pairs of fronts have been found as well. Their localization mechanism is, however, quite different from that discussed here; while in those equations the coupling of the two fields arises through reaction terms, it involves gradient terms in the extended Ginzburg-Landau equations discussed here.

The organization of the paper is as follows. In sec.II the extended Ginburg-Landau equations are discussed. The equations describing the interaction of fronts are derived in sec.III. They are analyzed in detail in sec.IV. In sec.V the effect of terms neglected in the derivation of the equations describing the interaction of the fronts is discussed using numerical simulations of the extended Ginzburg-Landau equations. In the concluding sec.VI we comment on the relevance of the concentration mode in combination with dispersion for understanding very recent experiments [21].

II. THE EXTENDED GINZBURG-LANDAU EQUATIONS

As shown in [31,32] the derivation of the conventional Ginzburg-Landau equations from the Navier-Stokes equations becomes invalid in the limit of vanishing mass diffusion of the second component. Since the Lewis number $\mathcal{L}$, which is given by the ratio of mass diffusion to heat diffusion, is $O(10^{-2})$ in liquids this implies that the conventional Ginzburg-Landau equation yields a poor description of the experimental system already for quite small convection amplitudes. Technically, in the limit $\mathcal{L} \to 0$ a certain concentration mode C cannot be eliminated adiabatically in favor of the traveling-wave amplitude A and has to be kept as an independent dynamical variable. For free-slip-permeable boundary conditions this leads to the following equations as a minimal model to capture the dynamics of the concentration mode [31],

$$\partial_{\tilde{t}}\tilde{A} + \tilde{s}\partial_{\tilde{x}}\tilde{A} = \tilde{d}\partial_{\tilde{x}}^2\tilde{A} + \tilde{a}\tilde{A} + \tilde{c}|\tilde{A}|^2\tilde{A} + \tilde{p}|\tilde{A}|^4\tilde{A} + \tilde{f}\tilde{C}\tilde{A}, \quad (1)$$

$$\partial_{\tilde{t}}\tilde{C} = \tilde{d}_c\partial_{\tilde{x}}^2\tilde{C} + \tilde{a}_c\tilde{C} + \tilde{h}\partial_{\tilde{x}}|\tilde{A}|^2 + \tilde{g}\tilde{C}|\tilde{A}|^2, \quad (2)$$

where the amplitude $\tilde{A}$ denotes the traveling-wave amplitude and is identical to that appearing in the conventional Ginzburg-Landau equation. The streamfunction $\tilde{\psi}$ and the deviations from the linear temperature profile as well as that from the concentration profile are therefore given by $(\tilde{\psi}, \tilde{\theta}, \tilde{\eta}) = \epsilon\tilde{A}e^{iq\hat{x}+i\omega\hat{t}}\sin\pi\hat{z}(\tilde{\psi}_0, \tilde{\theta}_0, \tilde{\eta}_0)$. The new concentration mode $\tilde{C}$ characterizes a long-wavelength mode of the concentration field which depends only on the vertical coordinate $\hat{z}$, $(\tilde{\psi}, \tilde{\theta}, \tilde{\eta}) = \epsilon C\sin 2\pi\hat{z}(0, 0, 1)$. From a more general perspective, eqs.(1,2) describe the interaction of a finite-wavenumber traveling wave with a zero-wavenumber steady mode. The interaction of two steady modes with very different wave numbers has been treated in [37].

To be precise, eqs.(1,2) do not contain all terms up to fifth order. The complete set up to third order including the values of the coefficients[1] for free-slip-permeable boundary conditions have been presented in [32]. Here we want to focus on the advection of C by the waves and the resulting feed-back on the traveling-wave amplitude through the dependence of its growth rate on the local (vertical) gradient in the concentration field. These important effects are described in eqs.(1,2) by the terms $\tilde{h}\partial_{\tilde{x}}|\tilde{A}|^2$ and $\tilde{f}\tilde{C}\tilde{A}$, respectively. In addition, the damping term $\tilde{a}_c\tilde{C}$ ($\tilde{a}_c < 0$) arises from vertical diffusion of the concentration. Through the term $C|A|^2$ this damping is also affected by convection. Note that eqs.(1,2) are only adequate if the convective amplitude is small enough to

[1] In [32] it had been overlooked that the coefficient h_4 has to vanish in general due to the fact that the concentration mode C is real [38].

satisfy $\tilde{a}_c + \tilde{g}|\tilde{A}|^2 < 0$. If this term were positive, plain waves $|A|^2 = A_0^2$ would be unstable to an evergrowing concentration mode. The leading-order contribution to the diffusive term $\partial_{\tilde{x}}^2 C$ does not arise from diffusion of the concentration; instead large-scale variations in the concentration field affect the local bouyancy of the fluid and generate vorticity which in turn advects the basic (linear) concentration profile.

To focus on the new localization mechanism, which was found numerically not to rely on the dispersive effects embodied in the imaginary parts of the coefficients [32], we consider here the special case in which all the coefficients and the amplitude A are real. In addition, to study the dynamics and interaction of fronts we restrict ourselves to the regime below threshold, $\tilde{a} < 0$. Eqs.(1,2) can then be simplified by introducing scaled variables *via*

$$A = \left(\frac{\tilde{p}}{\tilde{a}}\right)^{1/4} \tilde{A}, \quad C = -\frac{\tilde{f}}{\tilde{a}}\tilde{C}, \tag{3}$$

$$t = -\tilde{a}\tilde{t}, \quad x = \sqrt{\frac{-\tilde{a}}{\hat{d}}}\tilde{x}, \quad \tilde{d} = \eta^2 \hat{d}, \tag{4}$$

$$s = \frac{\tilde{s}}{\sqrt{-\tilde{a}\hat{d}}}, \quad c = \frac{\tilde{c}}{\sqrt{\tilde{a}\tilde{p}}}, \quad \delta = \frac{\hat{d}_c}{\tilde{d}}, \tag{5}$$

$$\alpha = \frac{\tilde{a}_c}{\tilde{a}}, \quad h = \frac{\tilde{h}\tilde{f}}{\sqrt{-\tilde{p}\tilde{a}^2\hat{d}}}, \quad g = \frac{\tilde{g}}{\sqrt{\tilde{a}\tilde{p}}}. \tag{6}$$

This leads to

$$\partial_t A + s\partial_x A = \eta^2 \partial_x^2 A - A + cA^3 - A^5 + CA, \tag{7}$$

$$\partial_t C = \delta \partial_x^2 C - \alpha C + h\partial_x A^2 + gCA^2. \tag{8}$$

Note that in the scaling (3-6) the reduced Rayleigh number $\tilde{a}$ has been scaled to -1. The parameter which allows a scanning between the Hopf bifurcation at $\tilde{a} = 0$ and the saddle-node bifurcation at $\tilde{a} = \tilde{c}^2/4\tilde{p}$ is now given by c. Its values range therefore from $c = 2$ at the saddle node to $c \to \infty$ at the Hopf bifurcation. For free-slip-permeable boundary conditions the coefficients α, δ, g and, in particular, h are positive [32]. In (4) we have introduced the parameter η. It characterizes the strength of the diffusion of the traveling-wave amplitude A and therefore governs the width of the fronts in A. In this paper we will consider the limit of narrow fronts, i.e. $\eta \ll 1$. This allows the derivation of equations describing the dynamics and interaction of fronts which focusses on the contribution from the concentration mode.

III. DERIVATION OF THE FRONT EQUATIONS

The goal of this paper is an analytical description of the contribution of the concentration mode to the interaction of fronts. In the standard approach to capture the interaction of fronts analytically one assumes the distance between the fronts to be large. The interaction, which is essentially due to the overlap of the fronts in the convective amplitude, is then weak and the resulting dynamics slow. In the present system the fronts interact additionally *via* the concentration mode. In certain parameter regimes the decay length of the concentration mode can be much larger than that of the convective amplitude. The interaction is then dominated by the concentration mode. Here we describe this regime by considering the limit of weak diffusion of A, $\eta \ll 1$. The fronts in A are then steep and the overlap between them can be ignored for any distance of O(1).

Based on numerical simulations [31,32] and a preliminary calculation for the interaction between widely separated fronts ($\eta = O(1)$) [39] we expect that stable pulses exist only if their velocity is opposite to the group velocity s (for $h > 0$). Since the difference between these two velocities has to be small in a perturbative approach we are led to assume, in addition, that the group velocity s is small, $s = \eta^2 s_2$. Consequently, the resulting (average) pulse velocity $v = (\partial_T x_R + \partial_T x_L)/2$ will also be small. Here $T = \eta^2 t$ is a slow time scale and x_R and x_L are the position of the front at the right and at the left end of the pulse, respectively. Finally, in order to obtain a manageable expression for the solution of (8) we assume

$$\delta = \eta^4 \delta_4, \quad \alpha = \eta^2 \alpha_2, \quad h = \eta^3 h_3, \quad g = \eta^2 g_2. \tag{9}$$

This amounts to assuming the concentration mode to be small and its diffusion and decay to be slow as compared to the velocity of the front. These scalings lead to

$$\partial_t A + \eta^2 s_2 \partial_x A = \eta^2 \partial_x^2 A - A + cA^3 - A^5 + CA, \tag{10}$$

$$\partial_t C = \eta^4 \delta_4 \partial_x^2 C - \eta^2 \alpha_2 C + \eta^3 h_3 \partial_x A^2 + \eta^2 g_2 C A^2. \tag{11}$$

Due to the smallness of the diffusion coefficient of A internal layers arise at the transitions from the conductive to the convective state. Thus, in the presence of two fronts the system has to be separated into five regions. This is sketched in fig.1. It shows also the typical shape of the fronts in the limit considered here. Whereas the traveling-wave amplitude is constant to lowest order in regions I, III and V, it changes rapidly from the conductive to the convective state in the transition regions II and IV. More precisely, in II and IV A and therefore also C varies on a fast space scale $y = \eta^{-1}x$. In order to match the solutions in the different regions the width 2Δ of regions II and IV needs to be small on the scale x but large on the scale y. This is achieved by taking $\Delta = \eta^{1/2}\Delta_{1/2}$.

The amplitudes A and C as well as the control parameter c are now expanded as

$$A = A_0 + \eta A_1 + ..., \quad C = \eta C_1 + ..., \quad c = c_0 + \eta c_1. \tag{12}$$

Here c is expanded around the value $c_0 \equiv 4/\sqrt{3}$ for which in the absence of the concentration mode the conductive and the convective state coexist, i.e. neither state invades

the other. In the transition regions II and IV one obtains then at $O(1)$

$$0 = \partial_y^2 A_0 + A_0 + c_0 A_0^3 - A_0^5. \tag{13}$$

At $O(\eta)$ and $O(\eta^2)$ one finds, respectively,

$$\partial_{T_1} A_0 + s_2 \partial_y A_0 = \left(\partial_y^2 + \mathcal{L}\right) A_1 + C_1 A_0 + c_1 A_0^3, \tag{14}$$

$$\partial_{T_1} C_1 = h_3 \partial_y A_0^2. \tag{15}$$

Here the intermediate time scale $T_1 = \eta t$ and the linearized operator $\mathcal{L} = 1 + 3c_0 A_0^2 - 5A_0^4$ have been introduced. Eq.(13) yields $A_0(y) = A_f((x_R - x)/\eta)$ in IV and $A_0(y) = A_f((x - x_L)/\eta)$ in II where the front solution is given by $A_f(\zeta) = A^* \left(\frac{1}{2}(1 + \tanh \zeta)\right)^{1/2}$ and $A^{*2} = \sqrt{3}$. Its position is given by x_R in IV and by x_L in II. Both can vary slowly in time, $x_{R,L} = x_{R,L}(T)$. Due to translational symmetry, the linearized operator $\partial_y^2 + \mathcal{L}$ is singular. Therefore eq.(14) leads to a solvability condition in each of the two regions. Thus, by projecting eq.(14) onto the left zero-eigenvector $\partial_y A_0$ one obtains evolution equations for x_R and for x_L, respectively. Note that in this approach the distance between the two fronts does not have to be assumed to be large in order to obtain two independent conditions. This is due to the small diffusion of A; any finite distance on the scale x is large on the relevant scale y.

Since A_0 depends on time only via $x_{R,L}(T)$ the general solution of eq.(15) in II and IV is given by

$$C_1 = k_1^{II,IV}(T) - \frac{h_3}{\partial_T x_{R,L}} A_0^2 \tag{16}$$

with $k_1^{II,IV}(T)$ being integration constants in the respective regions. Note that this solution is only valid as long as $\partial_T x_{R,L}$ is $O(1)$ or larger. For smaller velocities and in particular for stationary pulses the solution of the concentration equation becomes more complicated, in particular when the diffusion of C becomes relevant.

In regions I, III and V the traveling-wave amplitude A is constant to lowest order. Therefore, the source term $\partial_x A_0^2$ in the equation for C becomes less important than the damping term $-\alpha C$. Thus, in these regions eqs.(10,11) lead at $O(1)$, $O(\eta)$ and $O(\eta^3)$, respectively, to

$$0 = A_0 + c_0 A_0^3 - A_0^5, \tag{17}$$

$$\partial_{T_1} A_0 = \mathcal{L} A_1 + C_1 A_0 + c_1 A_0^3, \tag{18}$$

$$\partial_T C_1 = -\hat{\alpha} C_1 \tag{19}$$

where we have introduced the renormalized damping coefficient

$$\hat{\alpha} \equiv \alpha_2 - g_2 A_0^2. \tag{20}$$

Note that for free-slip-permeable boundary conditions one obtains $g_2 > 0$ [32], i.e. the damping is reduced by convection. The solution of eq.(17) is given by the extremal values of the front solution A_f. Since $\mathcal{L}$ is nonzero in the regions in question, eq.(18) can always be solved for A_1 and no solvability conditions arise in these regions. Eq.(19) has the general solution

$$C_1 = \tilde{C}_1(x) e^{-\hat{\alpha} T} \tag{21}$$

with the amplitude $\tilde{C}_1(x)$ as yet undetermined. Note that in the present scaling the concentration mode decays only due to damping; the diffusive term is irrelevant despite the fact that C can vary on O(1) length scales.

To make use of the solvability conditions the integration constants $k_1^{II,IV}$ appearing in the solution for C_1 in II and IV are needed. They are obtained by matching the solutions in the different regions. In the limit of weak diffusion considered here ($\delta \ll 1$) the solution depends qualitatively on the direction of propagation of the two fronts. In the following we concentrate on the case in which the two fronts travel in the same direction and can therefore form a bound pair. If they travel towards each other no interesting interaction arises in this limit. For fronts traveling away from each other the calculation would have to be modified. For concreteness we assume both $v_R \equiv \partial_T x_R$ and $v_L \equiv \partial_T x_L$ to be positive.

The traveling-wave amplitude vanishes in I and V and in III one has $A_0 = A^*$. Due to the damping term αC, the concentration mode vanishes also far ahead of the pulse, i.e. in V, . This implies $k_1^{IV} = 0$. At the right end of region III C_1 is therefore given by

$$C_1(x_R - \Delta, T) = -\frac{h_3}{v_R(T)} A^{*^2}. \tag{22}$$

To obtain C_1 at the left end of region III at time t, i.e. at $x_L(T) + \Delta$, one has to take into account that the concentration field at that location has been generated by the leading edge of the pulse (which is now at $x_R(T)$) at an *earlier* time $T^r \equiv T - \Delta T$ and has suffered an exponential decay since then. Thus one obtains

$$C_1(x_L + \Delta, T) = -\frac{h_3}{\partial_T x_R(T - \Delta T)} A^{*^2} e^{-\hat{\alpha}\Delta T}, \tag{23}$$

where the delay ΔT is determined by

$$x_R(T - \Delta T) = x_L(T). \tag{24}$$

Thus, in region II the concentration field C_1 is given by

$$C_1 = h_3 A^{*^2} \left\{ \frac{1}{v_L(T)} (1 - \frac{A_0^2}{A^{*^2}}) - \frac{1}{v_R(T - \Delta T)} e^{-\hat{\alpha}\Delta T} \right\}. \tag{25}$$

For the solvability conditions C_1 need not be determined in region I.

Projecting eq.(14) onto $\partial_y A_0$ leads in region II and IV, respectively, to the equations

$$v_L(T) = s_2 - \frac{\gamma}{v_L(T)} + \frac{2\gamma e^{-\hat{\alpha}\Delta T}}{v_R(T-\Delta T)} - \rho, \tag{26}$$

$$v_R(T) = s_2 - \frac{\gamma}{v_R(T)} + \rho, \tag{27}$$

$$\partial_T L = v_R(T) - v_L(T) \tag{28}$$

with $L = x_R - x_L$ and

$$\gamma = \sqrt{3}h_3, \quad \rho = \sqrt{3}c_1. \tag{29}$$

Here we have used

$$\int_{-\infty}^{\infty} \left(\partial_y A_0\right)^2 dy = A^{*2}/4 = \sqrt{3}/4. \tag{30}$$

In terms of the front velocities $v_{R,L}(t)$ the delay ΔT is given by

$$\int_{T-\Delta T}^{T} v_R(T')dT' = L(T). \tag{31}$$

Thus, in the general case, in which v_R depends on time, eqs.(26,27) with (31) represent a set of implicit integral-delay equations. In the present scaling of weak diffusion, however, the dynamics in region IV is decoupled from that in region II. Therefore v_R is constant and the retarded velocity $v_R(T-\Delta T)$ is equal to v_R. Consequently, the delay is given by $\Delta T = L/v_R$ and one obtains

$$v_R = s_2 - \frac{\gamma}{v_R} + \rho, \tag{32}$$

$$v_L(T) = s_2 - \frac{\gamma}{v_L(T)} + \frac{2\gamma e^{-\hat{\alpha}L/v_R}}{v_R} - \rho, \tag{33}$$

$$\partial_T L = v_R - v_L(T). \tag{34}$$

The results for negative front velocities are obtained in a similar way. Both can be combined into equations for the velocities $v_{l,t}$ of the leading and the trailing front, respectively,

$$v_l = s_2 - \frac{\gamma}{|v_l|} + sgn(v_l)\rho \tag{35}$$

$$v_t = s_2 - \frac{\gamma}{|v_t|} + 2\gamma\frac{e^{-\hat{\alpha}L/|v_l|}}{|v_l|} - sgn(v_t)\rho, \tag{36}$$

$$\partial_T L = \gamma\left(\frac{1}{v_t} - \frac{1}{v_l}\right) - 2\gamma\frac{e^{-\hat{\alpha}L/|v_l|}}{v_l} + 2\rho. \tag{37}$$

Here we have used $\partial_T L = sgn(v_l)(v_l - v_t)$ which assumes that both fronts travel in the same direction. Note that eq.(37) does not represent a closed equation for $L(T)$ due to the dependence of v_t on L. The equation for v_t is quadratic in v_t and contains in addition the sign of v_t, $sgn(v_t)$. Elimination of v_t in favor of L would therefore lead to complicated expressions involving the exponential within square roots. We therefore prefer to discuss eqs.(35,36) for the velocities instead of the equation for $L(T)$.

It should be pointed out that the validity of eqs.(36,37) is not limited to large values of L. Therefore $\gamma e^{-\hat{\alpha}L/|v_l|}$ can be of the same order as γ itself. In the present scaling the traveling-wave amplitudes A of the two fronts do not overlap on this length scale and do therefore not contribute to their interaction. We will comment on the possible consequences of an overlap in A and of dispersion at the end of sec.V.

IV. DISCUSSION OF THE FRONT EQUATIONS

In the limit $L \to \infty$ eqs.(35,36) describe the dynamics of a single front. More precisely, a single front connecting the state $A = A^*$ for $x \to -\infty$ with the state $A = 0$ for $x \to +\infty$ corresponds in the present calculation to a leading front for $v > 0$ (cf. fig.2a) and to a trailing front for $v < 0$ (cf. fig.2b). Its velocity v is therefore given by the relationship

$$\rho = v + \frac{\gamma}{|v|} - s_2 \tag{38}$$

or equivalently by

$$v = \frac{1}{2}\left(s_2 + \rho \pm \sqrt{(s_2+\rho)^2 - 4sgn(v)\gamma}\right). \tag{39}$$

Fig.3 gives a typical behavior of v as a function of ρ for such a front. It clearly exhibits a hysteretic transition from a 'fast' front to a 'slow' front when decreasing ρ from positive values through the saddle-node bifurcation at

$$\rho_{SN} = 2\frac{\gamma}{\sqrt{|\gamma|}} - s_2. \tag{40}$$

It is expected that only fronts on the top and on the bottom branch are stable and those on the middle branch are unstable. Since the main difference between the fast and the slow front is the strength of the concentration mode the destabilizing mode of fronts on the middle branch will mainly involve the concentration mode.

The possibility of a hysteretic transition between fast and slow fronts is not unexpected. The source of the concentration field is given by the gradients of the traveling front in the traveling-wave amplitude. If the front is traveling fast, the source remains at any given location only briefly and therefore generates only a weak concentration field which in turn has only little effect on the propagation velocity of the front. If the front is slow, however, a strong concentration field can be built up which slows down the front considerably providing a positive feedback mechanism. Note that, in experiments, increasing ρ corresponds to increasing the Rayleigh number. Thus, in principle it may be possible to observe this drastic manifestation of the concentration mode experimentally.

A right-traveling front connecting $A = A^*$ for $x \to -\infty$ with $A = 0$ for $x \to +\infty$ is not equivalent to one connecting $A = 0$ with A^* traveling to the left (cf. fig.2c).

This is due to the fact that A is the amplitude of right-traveling convection rolls. Reflection in space therefore yields left-traveling rolls with opposite group velocity s and opposite advection of the concentration field, $h\partial_x A^2$. The velocity of such a front is obtained from eq.(39) by flipping the sign of ρ. The velocities for both types of fronts are shown in fig.4. In contrast to fig.3 the velocity of the leading front is now marked by heavy solid lines and that of the trailing front – in the limit $L \to \infty$ – by thin dashed lines. For $\rho = 0$ the convective and the conductive state have the same energy in this dispersionless case. In the absence of any interaction the trailing and the leading front have therefore the same velocity. Due to reflection symmetry the concentration field affects the velocity of both types of fronts in the same way. Thus, $v_l(\rho)$ and $v_t(\rho, L \to \infty)$ intersect at $\rho = 0$ even in the presence of the concentration field, as indicated by the three open circles. These three solutions at infinite L imply the existence of three different localized waves (pulses) within this framework.

At finite distances the fronts interact with each other. Fig.4 shows the somewhat complicated behavior arising from the interaction. The broken lines give the velocity v_t of the trailing front as a function of ρ and with the velocity v_l determined correspondingly. The parameters are given by $\gamma = 0.15$, $\alpha = 0.01$, $g = 0$ and $s = 1$. The distance between the fronts is $L = 10$ in fig.4a and $L = 30$ in fig.4b. Eq.(36) is quadratic in v_t. One therefore obtains up to two solutions for given v_l, ρ and L, i.e. the curve $v_t(\rho)$ can split up into two branches. Eqs.(35,36) are, however, only valid if v_t and v_l have the same sign. Thus, for $v_t < 0$ only one branch remains which is marked by heavy short dashes. Due to the interaction it is shifted to smaller values of ρ. Consequently, the intersection of v_l and v_t, which signifies a pulse solution, occurs for $\rho < 0$. For $v_t > 0$ both branches are relevant. They are marked by heavy dashed and dotted-dashed lines, respectively. Due to the double-valued nature of v_l one obtains four different values of v_t for a given value of ρ, which are associated in a pairwise manner with the upper and the lower branch of v_l, respectively. Pulse solutions are given by the intersection points of the curves. Therefore, care has to be taken which value of v_t is associated with which branch of v_l. The relevant intersections are marked by solid circles.

The dependence of the velocity curves on the length L allows conclusions about the character of the interaction. For pulse A in fig.4 it is repulsive; without interaction (thin, dashed line) the magnitude of v_t would be larger than that of v_l and the trailing front would catch up with the leading front. With decreasing distance L, however, the interaction strength increases and the magnitude of v_t is reduced. Thus, the trailing front will approach the leading front until their velocities match. If the distance were to be decreased further, the trailing front would start lagging behind until the equilibrium distance is reached again. This suggests that the repulsive interaction leads to a stable pulse. By contrast, for pulse B the interaction is attractive and should render it unstable: the closer the trailing front comes to the leading front the faster it travels. For pulse C the interaction is again repulsive.

The above expectations about the stability of the pulses are borne out in a direct linear stability analysis. A linearization of eqs.(35-37) around the steady pulse solution with velocity v_0 and length L_0 (and corresponding delay $\Delta T_0 = L_0/v_0$) yields for the growth rate σ of perturbations

$$\sigma = -\frac{2\hat{\alpha}}{1 - \frac{v_0|v_0|}{\gamma}} e^{-\hat{\alpha} L_0/|v_0|}. \tag{41}$$

For $\hat{\alpha} > 0$ the pulses are therefore stable as long as $v_0|v_0|\gamma^{-1} < 1$[2]. The saddle-node bifurcation of the leading pulse occurs at $v_0|v_0| = \gamma$. This stability result corresponds therefore to the two cases with repulsive interaction discussed above (A and C). Only the case $v_0 < 0$ will lead to stable pulses since on the lower branch ($0 < v_0|v_0| < \gamma$) the leading front itself is unstable to perturbations in the concentration field which take it either to the fast or to the slow branch. This instability is not contained in the present analysis of the velocity and interaction of fronts (eqs.(35,36)), since it involves a change in the character of the front which is not merely given by a change in its position.

Can one understand the stability of backward traveling pulses intuitively? Consider the experimentally relevant case $\gamma > 0$ [32]. Then the negative gradient of A^2 at the right front leads to a negative peak of C whereas the left front generates a positive peak. If the pulse is stationary, both peaks have the same magnitude due to reflection symmetry as indicated in fig.1 by the dotted line. At the right front the concentration field reduces the local growth rate of A and therefore pushes the pulse to the left. Similarly, the peak at the left front enhances the growth rate und also pushes the pulse to the left. Thus, in the stationary case both peaks change the pulse velocity by the same amount and therefore do not contribute to the interaction. If the pulse travels, however, this is not the case any more. For negative velocities both peaks become steeper to their left side and much shallower to the right (dashed line), and the concentration field of the left front influences the right front much more than the other way around. Thus, while the left front enters a region with $C = 0$, the right front propagates into a region with $C > 0$. The magnitude of the concentration field at the right front is therefore reduced as indicated by heavy lines in fig.1. Consequently, the right front is pushed less to the left than the left one resulting in a repulsive interaction. This argument shows that to lowest order the stability of the pulses requires that their

[2]Note that for $\hat{\alpha} < 0$ the basic equations (1,2) are not appropriate.

velocity v be opposite to the group velocity s: they travel *backwards*.

The dependence of the length of the stable pulse on ρ is shown in fig.5. As expected the length diverges at $\rho = 0$. It monotonically decreases with increasing $|\rho|$. Strikingly, within this framework the stable pulse exists for arbitrarily large negative values of ρ. To wit, for large ρ and small v_l the velocity and length are given to leading order by

$$v_l = \gamma/\rho + ..., \quad L = \frac{s_2}{\gamma\alpha}\frac{1}{\rho^2} + ..., \tag{42}$$

implying that the repulsive interaction becomes arbitrarily large in this limit. This is due to the prefactor $1/v_l$ in eq.(36): with decreasing magnitude of the velocity the build-up of the concentration field becomes stronger and stronger. By contrast, for the (attractive) interaction of fronts in the real Ginzburg-Landau equation alone the prefactor of the exponential is constant and the strength of the interaction remains bounded.

V. NUMERICAL RESULTS

In the derivation of (35,36) we have pushed the diffusion of A as well as the diffusive term in C to higher order. To get an impression of the influence of these effects on single fronts and pulses we investigate eqs.(7,8) numerically. In fig.6 the results for the velocity v of a single front are given as a function of $c \equiv (4+\eta\rho)/\sqrt{3}$ for increasing values of δ [40]. The large symbols denote the velocity of a left-front, i.e. a front connecting $A(x \to -\infty) = 0$ with $A(x \to +\infty) = A^*$, whereas the small open circles denote that of a right-front. These results show that the singularity in $c = c(v)$ at $v = 0$ for a single front disappears when the diffusive term for C is included; instead the slow fronts on the bottom branch also undergo a saddle-node bifurcation and the two branches, which are separated in the approximation leading to eqs.(35,36), are connected in an S-shaped curve. With increasing δ the S-shape becomes less pronounced and one obtains eventually a continuous transition to a single-valued velocity. A similar transition occurs with decreasing coupling strength.

The diffusive terms have also a strong effect on the regime of existence of the stable pulse. The results of numerical simulations of eq.(7,8) are shown in fig.8(a,b) which give the length L and the velocity v of the pulse as a function of c for different values of δ. While the length appears to diverge with increasing c, the pulses disappear in a saddle-node bifurcation at small values of c.

This behavior can be understood qualitatively in the following way. In the presence of diffusion not only the trailing but also the leading front is affected by the interaction. For very weak diffusion, the effect on the leading front will, however, be negligible. Nevertheless, the solution branches cannot be separated into trailing and leading fronts any more. Instead one has to label them again as left and right fronts with velocities v_L and v_R. Considering the diffusionless result, we expect that for weak diffusion the stability of the pulses requires that their velocity be negative and that the isolated left-front be slower than the right-front. Therefore, c must be larger than a minimal value c_{min} at which v_L vanishes and below a maximal value c_{max} at which $v_L = v_R$. This is sketched in fig.7. The difference Δv in the velocities has to be compensated by the interaction term, which will now also depend on δ. Keeping the main ingredients of the interaction in mind one may expect it to be of the form $f(v)e^{-\hat{\alpha}L/|v|}$ where $f(v)$ remains now bounded for $v \to 0$. Balancing the two terms one obtains the relationship $L = -\hat{\alpha}^{-1}|v| \ln(\Delta v/f(v))$. Thus, if $\Delta v \to 0$ at finite v the length diverges. This is the case at c_{max}. If, however, $v \to 0$ at finite Δv, as is the case at c_{min}, $L \to 0$.

Of course, when L reaches $O(\eta)$ the overlap in the traveling-wave amplitude A has to be taken into account, as well. Since for very small lengths all pulse-like initial conditions will collapse, a short, unstable pulse has to exist which separates the basins of attraction of the pulseless solution ($A = 0$) and that of the stable pulse. With decreasing c the stable pulse is therefore expected to collide with this unstable pulse in a saddle-node bifurcation for c slightly above c_{min}. The unstable pulse should correspond to that of the uncoupled real Ginzburg-Landau equation where it exists for $c > c_{max}$ and has diverging length for $c \to c_{max}^+$. In the presence of the concentration mode it appears to be created together with the stable pulse already for $c < c_{max}$ at a finite length.

With increasing δ - and also with decreasing h - the hysteresis in the front velocities decreases. The range (c_{min}, c_{max}) will therefore decrease and vanish above some critical value of δ. Thus, stable pulses exist only for sufficiently strong coupling h and sufficiently weak diffusion δ (cf. fig.8)).

In principle, it is conceivable that the left-front solution reaches its saddle-node bifurcation at negative v_L. In that case the branch of stable pulses has to cease because no suitable leading front exists. The length at which this occurs could be sufficiently large that the overlap in A is irrelevant and may diverge with increasing δ or decreasing h.

VI. CONCLUSION

In this paper we have investigated the dynamics of fronts which interact via a long-wavelength mode. The work was motivated by convection in binary liquid mixtures where the fronts connect the motionless state with the convective state and the long-wavelength mode corresponds to a concentration mode which arises due to small mass diffusion. We have shown that this additional mode can lead to stable pulses in the form of bound pairs of fronts even in the absence of dispersion.

How do these results relate to experiments in binary-mixture convection? Of course, the physical system is not dispersionless, i.e. the coefficients in equation (1) as well as the traveling-wave amplitude are in general complex. It has been shown previously [29,30] that this by itself can lead to stable bound pairs of fronts without the presence of a concentration mode. For weak dispersion one obtains an equation of the form [29,30]

$$\partial_T L = k_1(c - c_0) - k_2 e^{-L/\xi} + \frac{k_3}{L} \tag{43}$$

for the length L of a pulse with k_1 and k_2 positive. The exponential term represents the attractive interaction between fronts due to the overlap of their exponential tails in the convective amplitude, while the algebraic interaction term arises from dispersion. For suitable parameters it can be repulsive ($k_3 > 0$). Within this framework, for $k_3 > 0$ and $c < c_0$ one has two pulse solutions as in the dispersionless case discussed above. Again the one with larger L is the stable one[3]. This ordering appears to persist for strong dispersion where the stable pulse may be identified with a dissipatively perturbed soliton solution of the nonlinear Schrödinger equation [41].

In recent experiments, both stable as well as unstable pulses have been investigated in great detail [21]. The unstable ones have been obtained by employing a suitable servo control. In that work two regimes have been found. For a value of the separation ratio of $\psi = -0.127$ two pulses exist for a given Rayleigh number and the stable pulse is the *shorter* one. For $\psi \leq -0.17$ the branch with the longer, unstable pulses turns around and one is left with a single pulse solution which is stable.

It is tempting to speculate that the experimental finding of longer, unstable pulses can be described by including dispersion as well as the concentration mode. The derivation of the relevant equations appears to be involved. Considering eqs.(43) and (35,36,37) one may expect that an equation of the form

$$\partial_T L = k_1(c - c_0) - k_2 e^{-L/\xi} + \frac{k_3}{L} - 2\frac{\gamma}{v_l} e^{-\hat{\alpha}L/|v_l|} \tag{44}$$

could capture the main aspects. With $\gamma > 0$ as before this equation allows four solutions of forward traveling pulses ($v_l > 0$). This is illustrated in fig.9 where the dL/dt is plotted as a function of L for two exemplary cases. Again the shortest pulse at $L = 0.25$ (marked by an open triangle) is unphysical. The unstable pulse A constitutes the separatrix between the pulseless conductive state and the state with a stable pulse (B). It has not been observed. We identify the experimentally observed pulses with the stable pulse B and the unstable pulse with pulse C. Thus, within the extended equations an unstable longer pulse can coexist with a shorter stable one as seen in the experiment. Reducing c slightly below c_0 leads to a second stable pulse (D). Since its length diverges as $c \to c_0$ it may be too long to be observed in the present experiments.

When $\gamma/v_l > 0$ is decreased towards 0 the two pulses B and C merge in a saddle-node bifurcation and - in particular for backward traveling pulses ($v < 0$) - one is left with the unstable pulse A and the stable pulse D. We identify this situation with that found in the experiments for $\psi < -0.17$. This interpretation is supported by the fact that in the experiments the stability of the long pulses changes very close to where their velocity changes sign. Within the present scenario one would expect the length scale for the long, stable pulses to be set by the decay length $\ell \equiv |v|/\hat{\alpha_2}$ of the concentration field. Since convection has a strong influence on the decay rate through $\hat{\alpha} = \alpha_2 - g_2|A_0|^2$, such an estimate requires more than the knowledge of the Lewis number and the measured velocity of the pulses. It is therefore not too surprising that taking α_2 alone instead of $\hat{\alpha}$ leads to an unreasonably short decay length ℓ. Clearly more detailed calculations are necessary to substantiate the discussion based on eq.(44) [42].

In this paper we have concentrated on localized solutions which can be considered as bound pairs of fronts, each of which forms a heteroclinic orbit in space. This requires, of course, a subcritical bifurcation. It is worth noting that numerical simulations of the extended Ginzburg-Landau equations (7,8) have shown that localized waves can also arise in the case of a supercritical bifurcation, for which no single fronts exist [32]. These pulses correspond to homoclinic orbits in space. So far, they have not been captured in any analytic description.

This work was supported by DOE through grant (DE-FG02-92ER14303) and by an equipment grant from NSF (DMS-9304397). H.H. was supported by a grant of the F.P.I. program Ref.AP90 09297081 (M.E.C.). H.R. thanks the Universidad de Navarra for its hospitality. We gratefully acknowledge helpful suggestions by W.L. Kath and discussions with V. Hakim and with P. Kolodner, who kindly shared his data with us prior to publication.

[3] In the regime in question eq.(43) has in fact three solutions. The third solution, which is formally stable within eq.(43), is, however, always confined to $L/\xi = O(1)$. This small distance between the fronts is inconsistent with the assumption of weak interaction between them since $k_2 = O(1)$. In fact, this solution is unphysical; as discussed in the previous section, the smallest pulse must be unstable.

[1] J. Hegseth, J. Vince, M. Dubois, and P. Bergé, Europhys. Lett. **17**, 413 (1992).
[2] D. Raitt and H. Riecke, Physica D (submitted).
[3] D. Raitt and H. Riecke, in *Spatiotemporal Patterns in Nonequilibrium Complex Systems*, Santa Fe Institute,

edited by P. Cladis and P. Palffy-Muhoray (Addison-Wesley, ADDRESS, 1993).
[4] J. Hegseth, C. Andereck, F. Hayot, and Y. Pomeau, Phys. Rev. Lett. **62**, 257 (1989).
[5] A. Simon, J. Bechhoefer, and A. Libchaber, Phys. Rev. Lett. **61**, 2574 (1988).
[6] M. Rabaud, S. Michalland, and Y. Couder, Phys. Rev. Lett. **64**, 184 (1990).
[7] M. Gorman, M. el Hamdi, and K. Robbins, Comb. Sci. and Tech (to appear).
[8] H. Riecke and H.-G. Paap, Phys. Rev. A **45**, 8605 (1992).
[9] R. Wiener and D. McAlister, Phys. Rev. Lett. **69**, 2915 (1992).
[10] P. Coullet, R. Goldstein, and G. Gunaratne, Phys. Rev. Lett. **63**, 1954 (1989).
[11] R. Goldstein, G. Gunaratne, and L. Gil, Phys. Rev. A **41**, 5731 (1990).
[12] R. Goldstein, G. Gunaratne, L. Gil, and P. Coullet, Phys Rev. A **43**, 6700 (1991).
[13] B. Caroli, C. Caroli, and S.Fauve, J. Phys. I **2**, 281 (1992).
[14] A. Bayliss, B. Matkowsky, and H. Riecke, in *Numerical Methods for Partial Differential Equations with Critical Parameters*, edited by H. Kaper and M. Garbey (Kluwer Academic Publishing, ADDRESS, 1992).
[15] A. Bayliss, B. Matkowsky, and H. Riecke, Physica D **74**, 1 (1994).
[16] A. Bayliss, B. Matkowsky, and H. Riecke, in *Pattern Formation: Symmetry Methods and Application*, edited by W. L. J. Chadam, M. Golubitsky and B. Wetton (Amer. Math. Soc., Providence, RI, 1994).
[17] E. Moses, J. Fineberg, and V. Steinberg, Phys. Rev. A **35**, 2757 (1987).
[18] R. Heinrichs, G. Ahlers, and D. Cannell, Phys. Rev. A **35**, 2761 (1987).
[19] P. Kolodner, D. Bensimon, and C. Surko, Phys. Rev. Lett. **60**, 1723 (1988).
[20] P. Kolodner, Phys. Rev. Lett. **66**, 1165 (1991).
[21] P. Kolodner, preprint (1994).
[22] W. Barten, M. Lücke, and M. Kamps, Phys. Rev. Lett. **66**, 2621 (1991).
[23] M. Lücke, W. Barten, and M. Kamps, Physica D (1992).
[24] P. Kolodner, Phys. Rev. E **48**, 4187 (1993).
[25] O. Thual and S. Fauve, J. Phys. France **49**, 1829 (1988).
[26] W. van Saarloos and P. Hohenberg, Physica D **56**, 303 (1992).
[27] L. Pismen, Phys. Rev. A **35**, 1873 (1987).
[28] B. Malomed and A. Nepomnyashchy, in *Nonlinear Evolution of Spatio-temporal Structures in Dissipative Continuous Systems*, edited by F. Busse and L. Kramer (Plenum Press, ADDRESS, 1991).
[29] B. Malomed and A. Nepomnyashchy, Phys. Rev. A **42**, 6009 (1990).
[30] V. Hakim and Y. Pomeau, Eur. J. Mech. B Suppl **10**, 137 (1991).
[31] H. Riecke, Phys. Rev. Lett. **68**, 301 (1992).
[32] H. Riecke, Physica D **61**, 253 (1992).
[33] H. Riecke, in *Spatio-temporal Organization in Nonequilibrium Stystems*, edited by S. Müller and T. Plesser (Projekt Verlag, Dortmund, 1992), pp. 222–223.
[34] H. Riecke (unpublished).
[35] M. Renardy and Y. Renardy, Phys. Fluids (submitted).
[36] A. Hagberg and E. Meron, preprint (1992).
[37] P. Metzener and M. Proctor, Eur. J. Mech. B **11**, 759 (1992).
[38] P. Kolodner and P. Hohenberg, priv. comm. .
[39] H. Herrero and H. Riecke (unpublished).
[40] H. Herrero and H. Riecke, J. Bif. and Chaos **4**, (1994).
[41] V. Hakim, P. Jakobsen, and Y. Pomeau, Europhys. Lett. **11**, 19 (1990).
[42] W.-J. Rappel and H. Riecke, (in preparation).

FIG. 1. Influence of the propagation of the pulse on the concentration field. A stationary pulse has symmetric concentration field (dotted line for C). In a propagating pulse (dashed line for C) the trailing peak of C is reduced leading to an effective repulsion between the fronts (see text).

FIG. 2. Sketches of leading and trailing fronts for $v > 0$ and $v < 0$. a) leading front with $v > 0$. b) trailing front with $v < 0$. c) trailing front with $v > 0$. d) leading front with $v < 0$.
ffi

FIG. 3. Dependence of the velocity of a single front on ρ.

FIG. 4. Velocity of a leading (solid line) and of a trailing front (dashed lines) as a function of ρ. Thin dashed lines denote v_t for $L \to \infty$. Thick dashed lines give v_t for $L = 10$ and $L = 30$, respectively.

FIG. 5. Dependence of the length of pulses on ρ.

FIG. 6. Numerical results for the velocity v of a single front on c. The parameter values are $s = 0.3$, $\eta^2 = 0.05$, $\alpha = 0.01$ and $h = 0.03$.

FIG. 7. Sketch of the influence of diffusion and damping of C on the velocities $v_{l,t}$ of fronts. Solid lines for $L \to \infty$, dashed line gives v_t for finite L.

FIG. 8. Numerical simulations of pulses with $s = 0.3$, $\eta^2 = 0.05$, $\alpha = 0.01$ and $h = 0.03$. The grid size is $\Delta x = 0.1$ and the time step is $\Delta t = 1$. The simulations ar done in a frame moving with the pulse.

FIG. 9. dL/dt as a function of L according to eq.(44). In this regime eq.(44) has up to 4 steady pulse solutions.

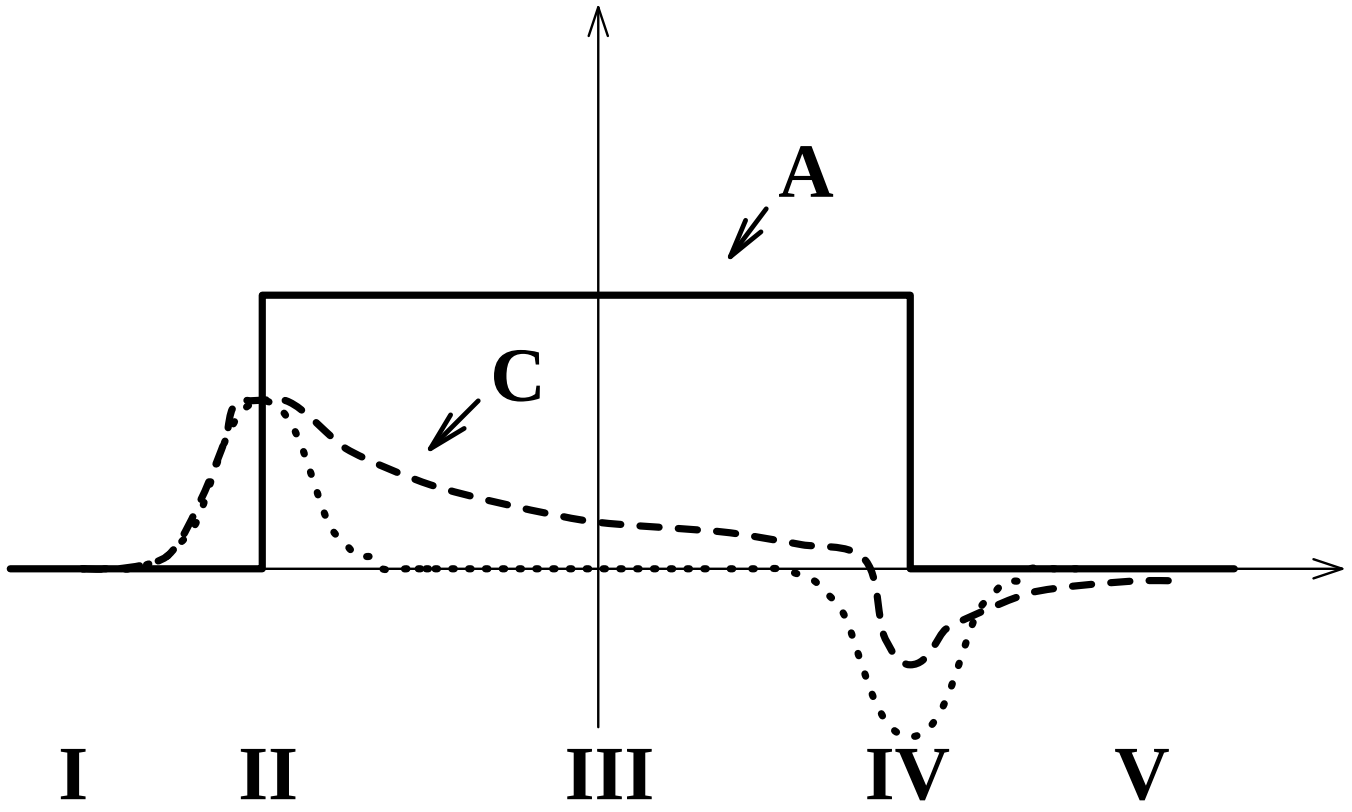
A
C
I
II
III
IV
V

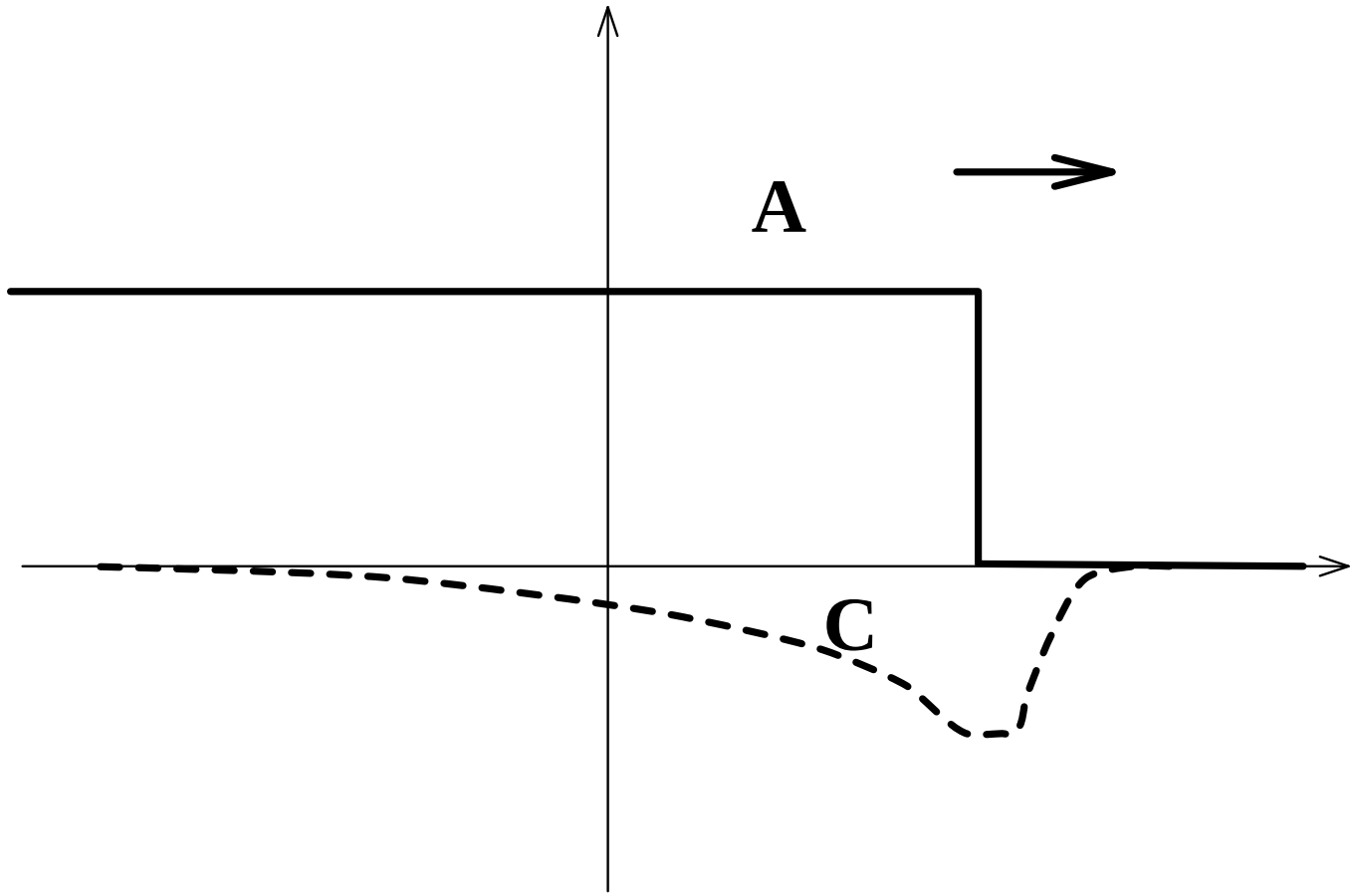
A
C

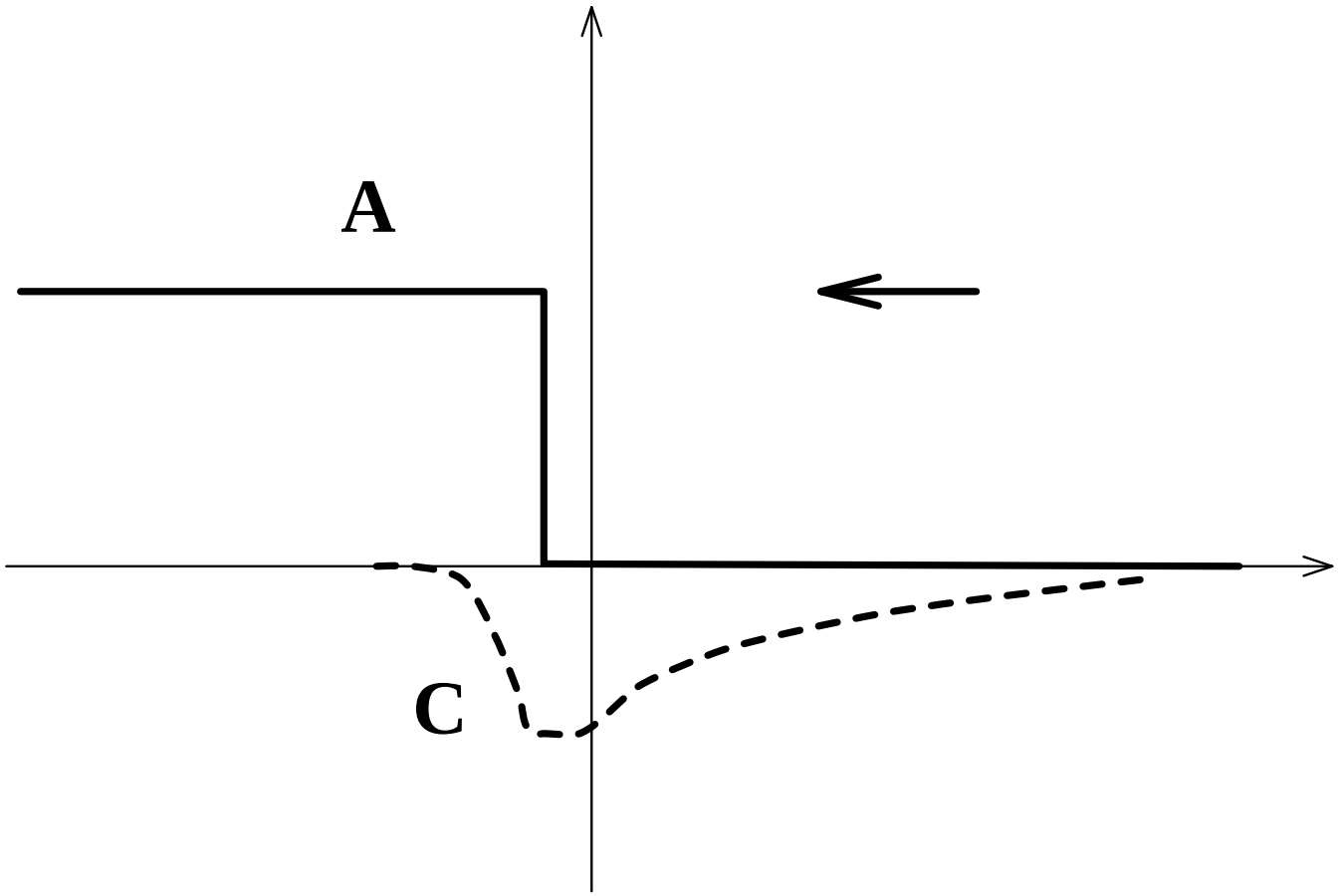
A
C

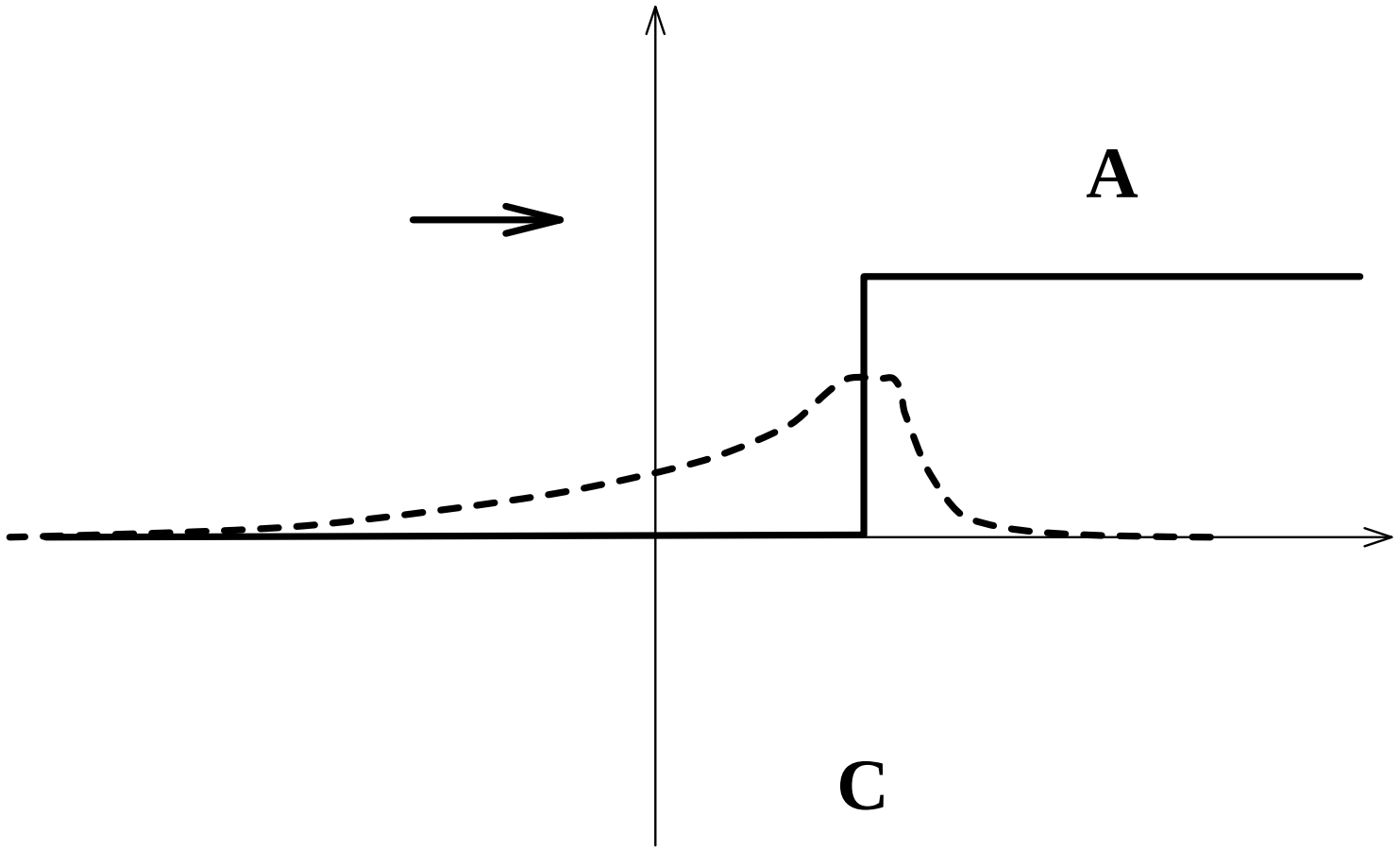
A
C

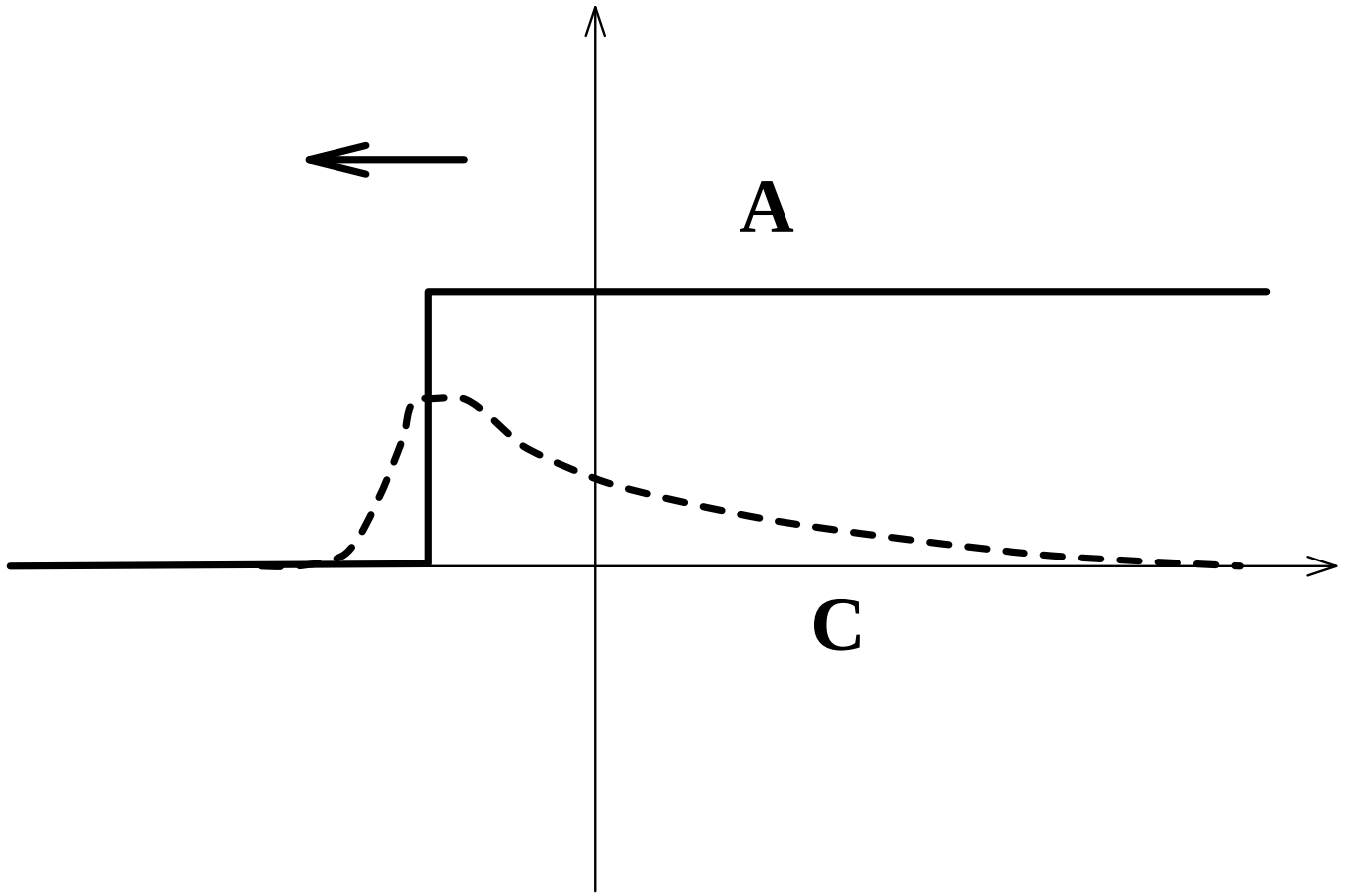
A
C

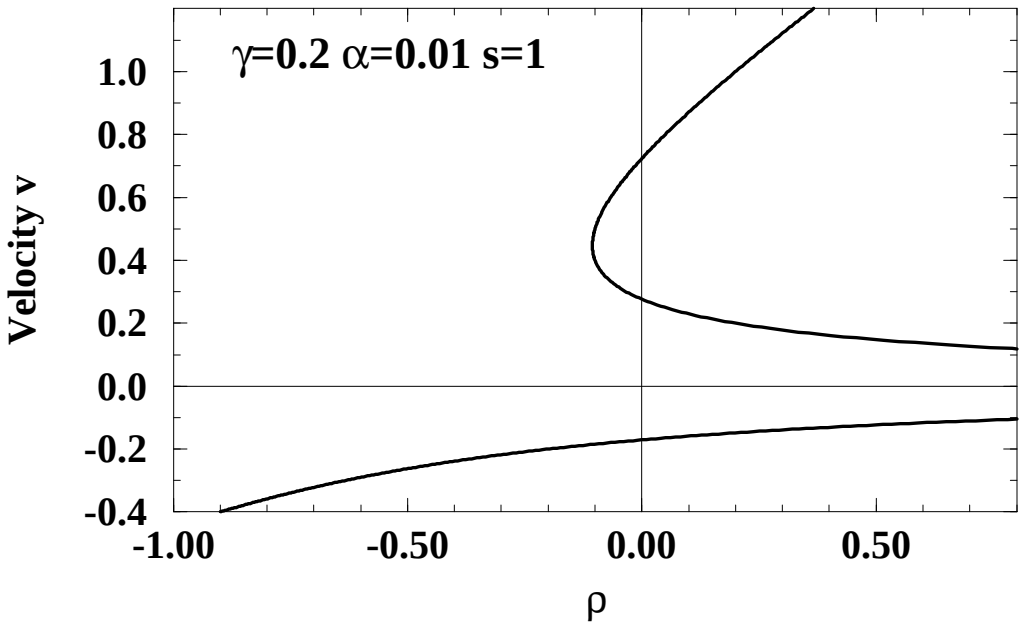
γ=0.2 α=0.01 s=1
Velocity v
1.0
0.8
0.6
0.4
0.2
0.0
-0.2
-0.4
-1.00
-0.50
0.00
0.50
ρ

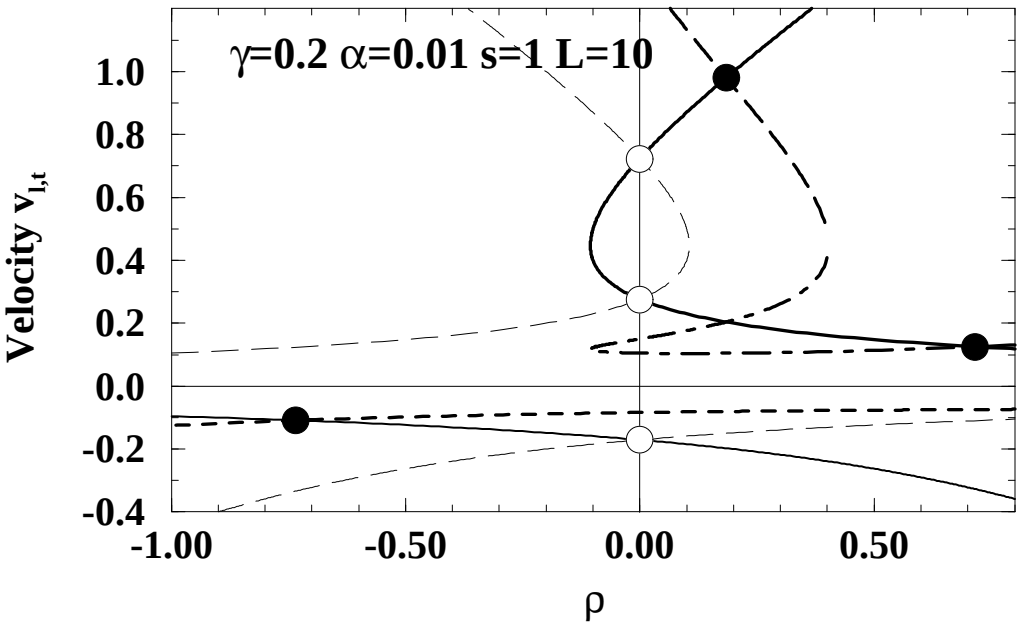
γ=0.2 α=0.01 s=1 L=10
1.0
0.8
0.6
0.4
0.2
0.0
-0.2
-0.4
Velocity v_{l,t}
-1.00
-0.50
0.00
0.50
ρ

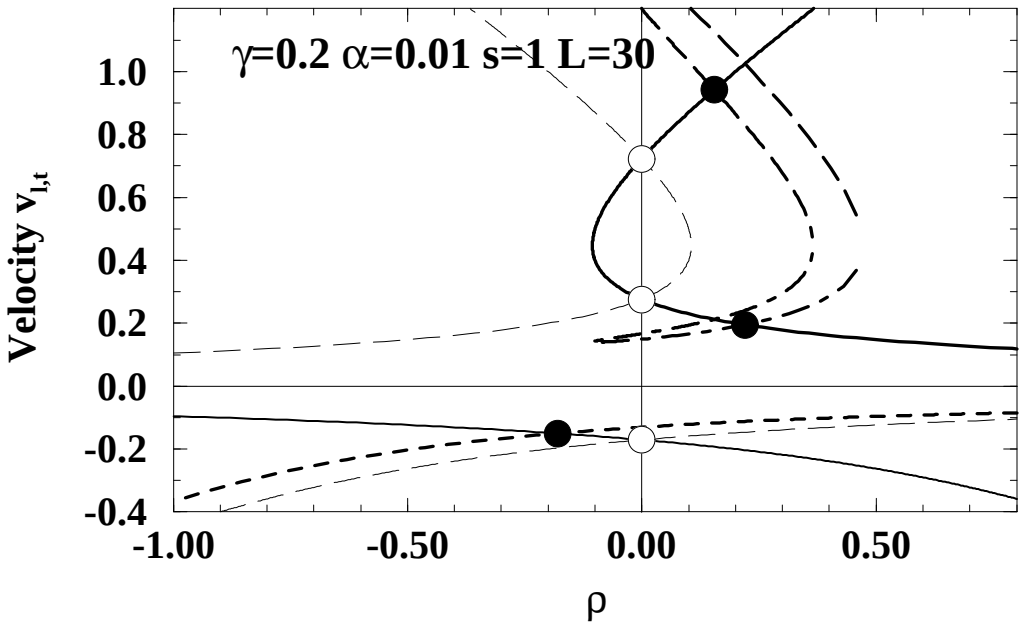
γ=0.2 α=0.01 s=1 L=30
Velocity v_{l,t}
1.0
0.8
0.6
0.4
0.2
0.0
-0.2
-0.4
-1.00
-0.50
0.00
0.50
ρ

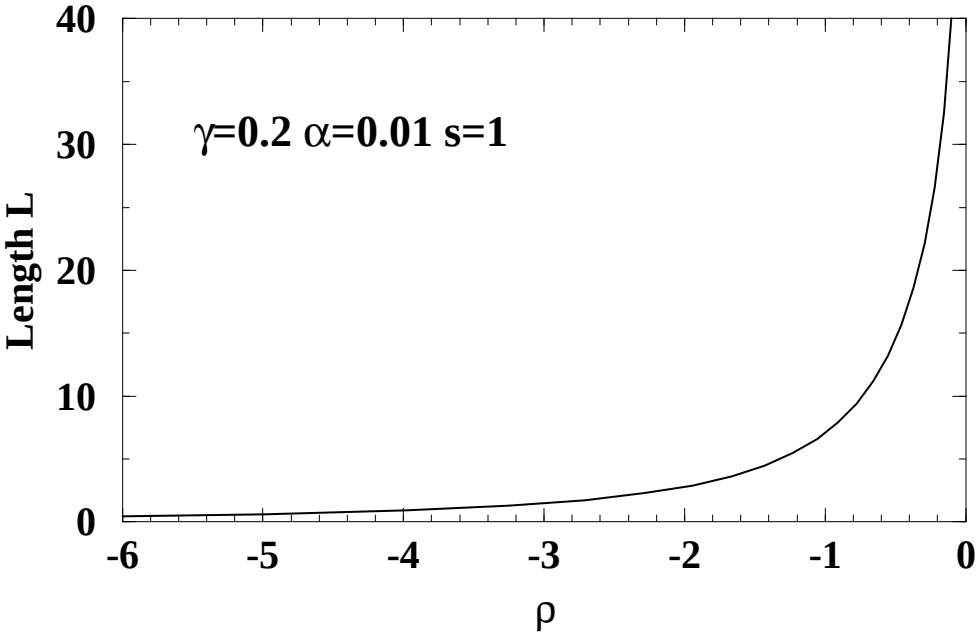
40
30
20
10
0
Length L
γ=0.2 α=0.01 s=1
-6
-5
-4
-3
-2
-1
0
ρ

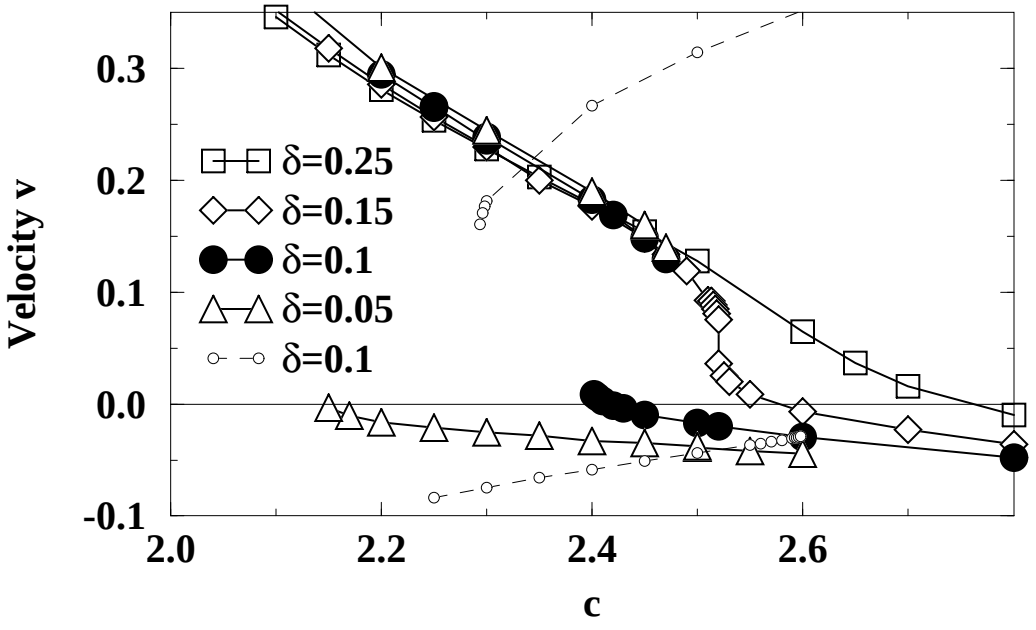
0.3
0.2
0.1
0.0
-0.1
Velocity v
δ=0.25
δ=0.15
δ=0.1
δ=0.05
δ=0.1
2.0
2.2
2.4
2.6
c

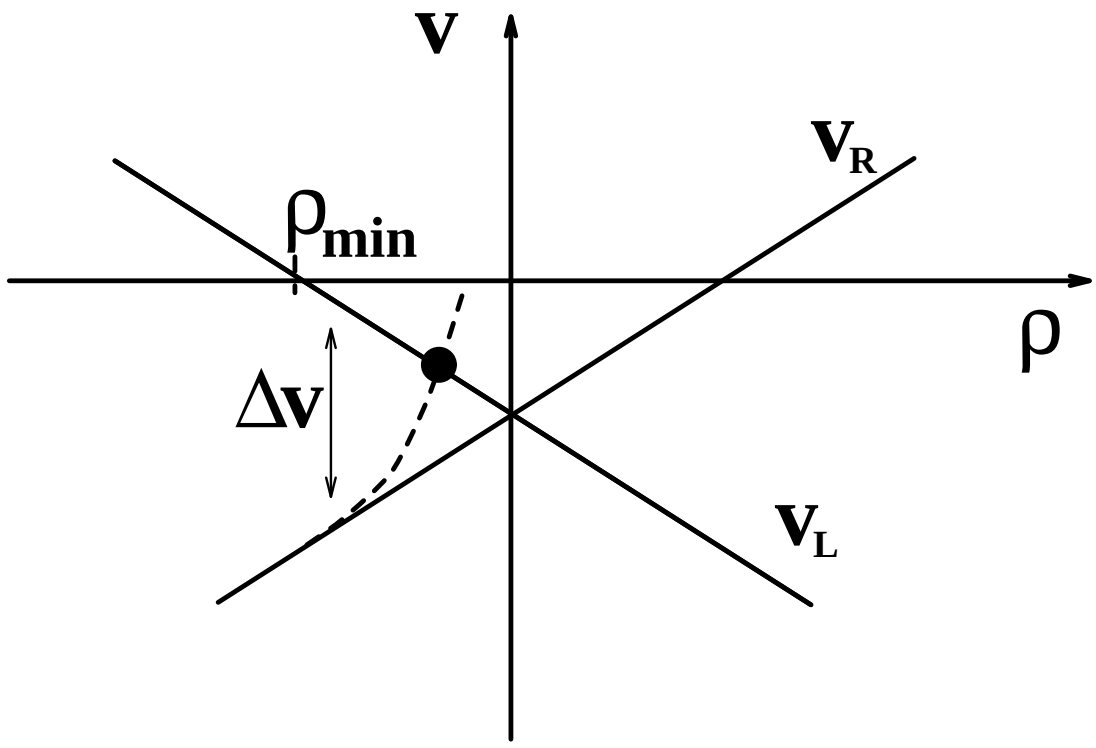
v
v_R
ρ_{min}
ρ
Δv
v_L

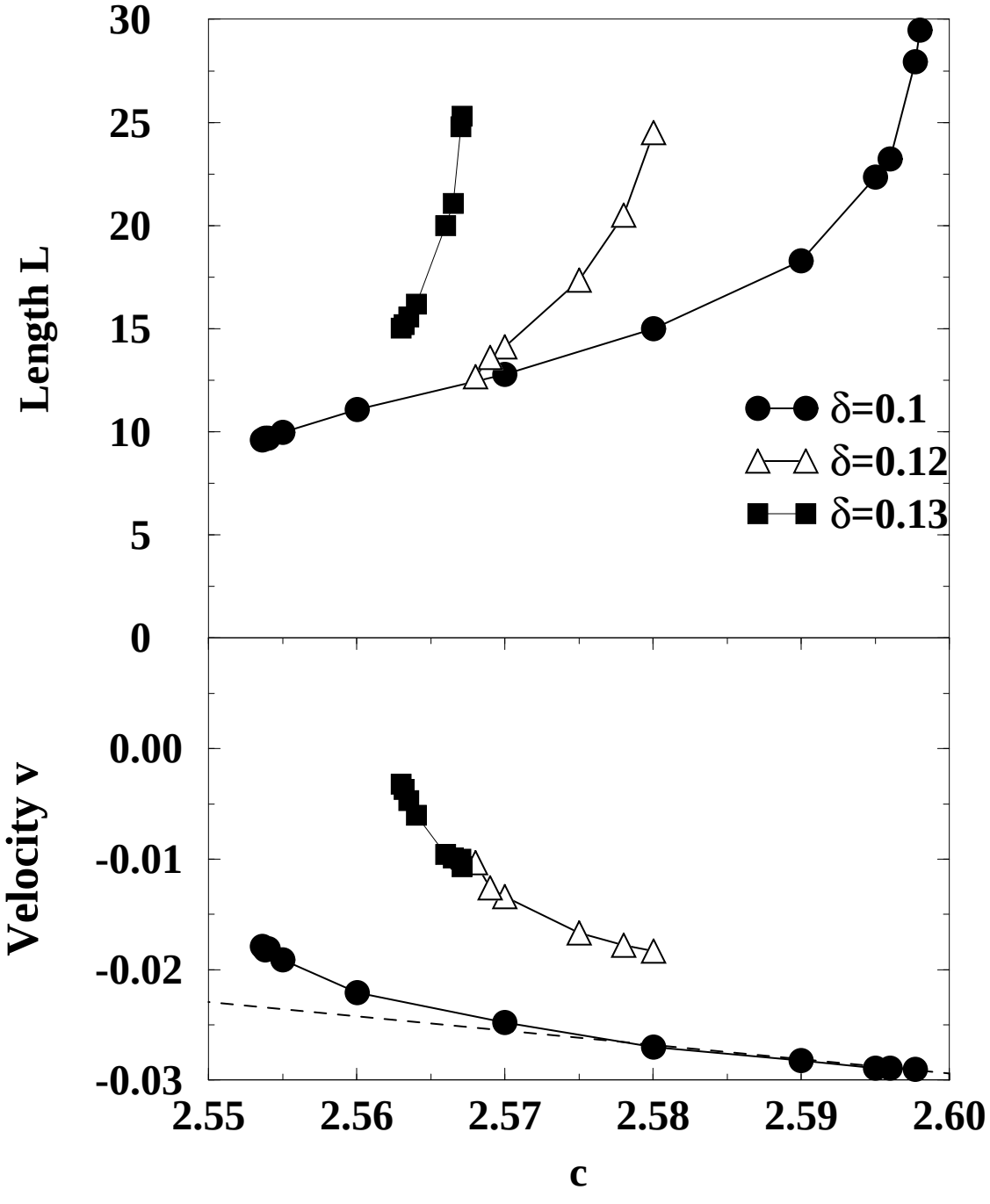
Length L
30
25
20
15
10
5
0
δ=0.1
δ=0.12
δ=0.13
Velocity v
0.00
-0.01
-0.02
-0.03
2.55
2.56
2.57
2.58
2.59
2.60
c

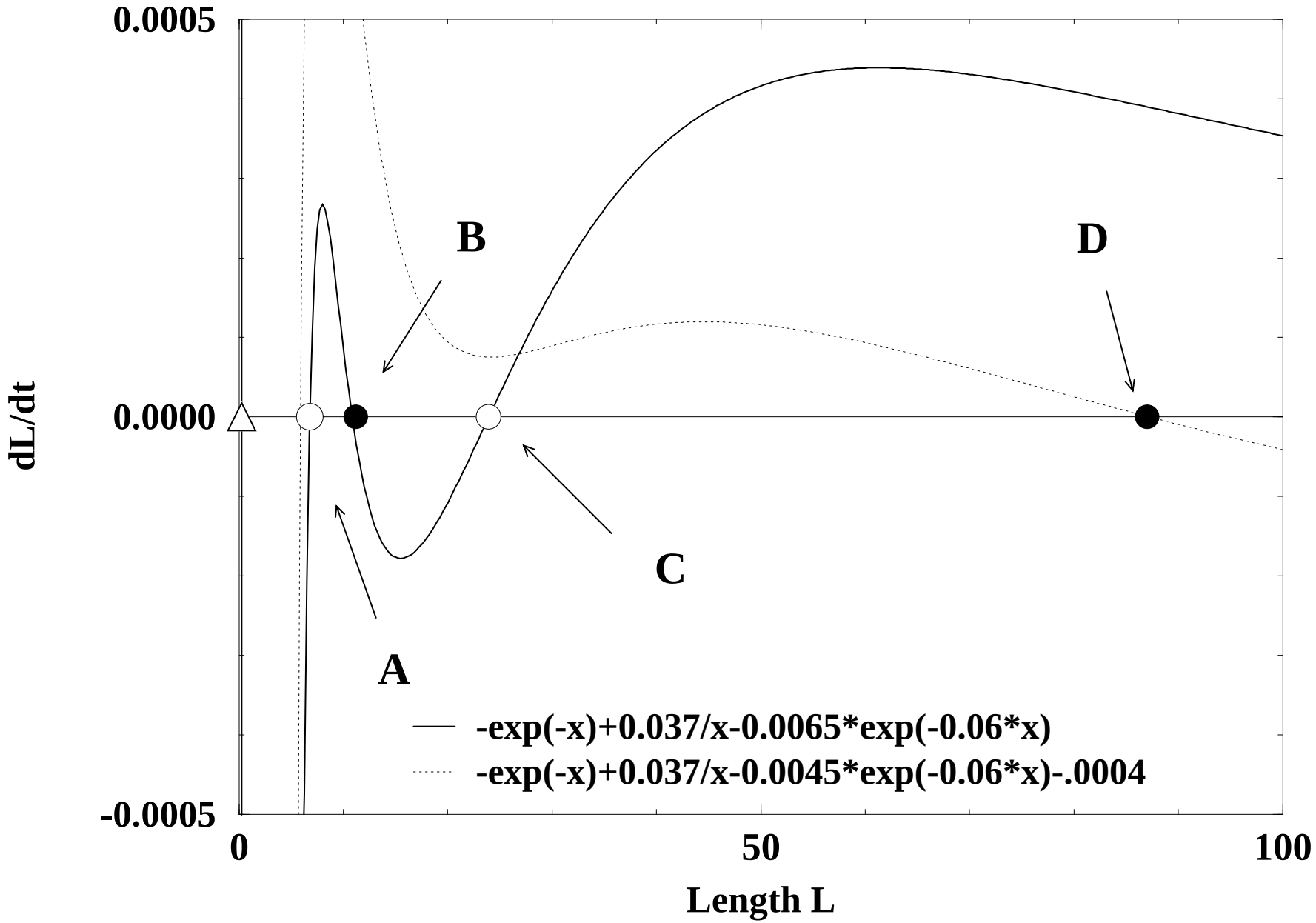
0.0005
0.0000
-0.0005
0
50
100
dL/dt
Length L
A
B
C
D
-exp(-x)+0.037/x-0.0065*exp(-0.06*x)
-exp(-x)+0.037/x-0.0045*exp(-0.06*x)-.0004